Research Letter DOI: 10.15541/jim20240035

Microstructure and Oxidation Behavior of ZrB_2-SiC Ceramics Fabricated by Tape Casting and Reactive Melt Infiltration

TAN Min[1,2], CHEN Xiaowu[1,2], YANG Jinshan[1,2], ZHANG Xiangyu[1,2], KAN Yanmei[1,2], ZHOU Haijun[1,2], XUE Yudong[1,2], DONG Shaoming[1,2]

(1. State Key Laboratory of High Performance Ceramics and Superfine Microstructure, Shanghai Institute of Ceramics, Chinese Academy of Sciences, Shanghai 200050, China; 2. Center of Materials Science and Optoelectronics Engineering, University of Chinese Academy of Sciences, Beijing 100049, China)

Abstract: ZrB_2-based ceramics typically necessitate high temperature and pressure for sintering, whereas ZrB_2-SiC ceramics can be fabricated at 1500 ℃ using the process of reactive melt infiltration with Si. In comparison to the conventional preparation method, reactive synthesis allows for the more facile production of ultra-high temperature ceramics with fine particle size and homogeneous composition. In this work, $ZrSi_2$, B_4C, and C were used as raw materials to prepare ZrB_2-SiC *via* combination of tape casting and reactive melt infiltration herein referred to as ZBC ceramics. Control sample of ZrB_2-SiC was also prepared using ZrB_2 and SiC as raw materials through an identical process designated as ZS ceramics. Microscopic analysis of both ceramic groups revealed smaller and more uniformly distributed particles of the ZrB_2 phase in ZBC ceramics compared to the larger particles in ZS ceramics. Both sets of ceramics underwent cyclic oxidation testing in the air at 1600 ℃ for a cumulative duration of 5 cycles, each cycle lasting 2 h. Analysis of the oxidation behavior showed that both ZBC ceramics and ZS ceramics developed a glassy SiO_2-ZrO_2 oxide layer on their surfaces during the oxidation. This layer severed as a barrier against oxygen. In ZBC ceramics, ZrO_2 is finely distributed in SiO_2, whereas in ZS ceramics, larger ZrO_2 particles coexist with glassy SiO_2. The surface oxide layer of ZBC ceramics maintains a dense structure because the well-dispersed ZrO_2 increases the viscosity of glassy SiO_2, preventing its crystallization during the cooling. Conversely, some SiO_2 in the oxide layer of ZS ceramics may crystallize and form a eutectic with ZrO_2, leading to the formation of $ZrSiO_4$. This leads to cracking of the oxide layer due to differences in thermal expansion coefficients, weakening its barrier effect. An analysis of the oxidation resistance shows that ZBC ceramics exhibit less increase in oxide layer thickness and mass compared to ZS ceramics, suggesting superior oxidation resistance of ZBC ceramics.

Key words: ultra-high temperature ceramic; ZrB_2-SiC; oxidation behavior; reactive melt infiltration

In recent years, hypersonic vehicles have become a key area of development in the aerospace sector of many countries due to the rapid advancement of aerospace technology and the urgent need to integrate air and space[1-3]. Certain vehicle segments, such as wing leading edges and nose cones, rub heavily against the atmosphere during long hypersonic cruises, trans-atmospheric flights, and atmospheric re-entries, generating extremely high temperatures[3-5]. Therefore, thermal protection materials for hypersonic vehicles must be physiochemically stable under high temperatures and oxidizing conditions for extended periods of time[6-8].

Received date: 2024-01-16; **Revised date:** 2024-03-04; **Published online:** 2024-03-30
Foundation item: National Key R&D Program of China (2022YFB3707700); Shanghai Science and Technology Innovation Action Plan (21511104800); National Natural Science Foundation of China (52172111); National Science and Technology Major Project (2017-IV-0005-0042); Key Research Program of the Chinese Academy of Sciences (ZDRW-CN-2021-2-2); Science Center for Gas Turbine Project (P2022-B-IV-001-001)
Biography: TAN Min (1998–), male, Master candidate. E-mail: tanmin21@mails.ucas.ac.cn
谭 敏(1998–), 男, 硕士研究生. E-mail: tanmin21@mails.ucas.ac.cn
Corresponding author: CHEN Xiaowu, associate professor. E-mail: xwchen@mail.sic.ac.cn;
DONG Shaoming, professor. E-mail: smdong@ mail.sic.ac.cn
陈小武, 副研究员. E-mail: xwchen@mail.sic.ac.cn; 董绍明, 研究员. E-mail: smdong@mail.sic.ac.cn

Current high-temperature structural materials comprise refractory metals, C_f/C composites, C_f/SiC composites, and ultra-high temperature ceramics[9]. Refractory metals such as tungsten (W) and rhenium (Re) were the first high-temperature resistant materials which had been studied and applied, but these materials have poor oxidation resistance and low specific strength and specific modulus[10]. In inert atmosphere, C_f/C composites can withstand temperatures above 3000 ℃. However, they are difficult to be used in oxidizing conditions above 500 ℃ due to their poor oxidation resistance[3,11-12]. In comparison to C_f/C composite materials, C_f/SiC composite materials have a significantly improved resistance to oxidation. However, they are also prone to rapid oxidation at temperatures above 1600 ℃[13]. Ultra-high temperature ceramics (UHTCs) are a class of materials with melting points above 3000 ℃, mainly composed of transition metal carbides and borides (ZrC, ZrB_2, HfC, HfB_2, *etc*). The characteristics of high strength, high hardness and high melting points, making them ideal for use in extreme aerospace environments[2, 4, 14].

ZrB_2 is considered to be a promising structural material for long-term use in extreme thermal environments due to its low theoretical density (6.09 $g\cdot cm^{-3}$) and high thermal conductivity (65–135 $W\cdot m^{-1}\cdot K^{-1}$) among ultra-high temperature ceramics[15-18]. ZrB_2-SiC ceramics, which are produced by the introduction of SiC into ZrB_2 ceramics, have excellent oxidation resistance at temperatures below 1500 ℃[19-20]. Due to their strong covalent bonding and low self-diffusion coefficient, ZrB_2-based ceramics require high-temperature and high-pressure sintering to form dense stacks[21-23]. Zhao *et al*.[24] sintered ZrB_2-20%(in vol)SiC by spark plasma sintering (SPS) at 1400, 1600 and 1800 ℃ to produce ceramics with different porosities, and these ceramics were tested for high temperature oxidation. The ceramics sintered at 1800 ℃ exhibited the best oxidation resistance, with the smallest change in the thickness of the ZrO_2-SiO_2 oxide layer. To lower the sintering temperature of ZrB_2 ceramics, Silvestroni *et al*.[25] utilized $ZrSi_2$, $MoSi_2$, $TaSi_2$, and WSi_2 as sintering aids, to obtain four kinds of ZrB_2 ceramics by hot press sintering respectively. The impact of these four sintering aids on the oxidation resistance of ZrB_2 ceramics was then investigated, and the results showed that $MoSi_2$ could significantly improve the oxidation resistance of ZrB_2 ceramics. The reason is that Mo increases the viscosity of glassy SiO_2, which leads to the inhibition of columnar ZrO_2 formation. Reactive melt infiltration can densify ceramics at lower temperatures compared to sintering aids, and without the need for pressure. D'amico *et al*.[26] produced ZrB_2-SiC ceramics by reactive melt infiltration of Si at 1500 ℃ under vacuum and studied the oxidation resistance of the ceramics oxidized at 1500 ℃ for 48 h. The results showed that the oxidation rate of ZrB_2-SiC ceramics prepared by reactive melt infiltration was slower than that of ceramics prepared by other methods. Compared with the conventional preparation method, it is easier to obtain ultra-high temperature ceramics with fine particle size and homogeneous composition by reactive preparation. Lee *et al*.[27] used $ZrSi_2$-B_4C-C as a sintering aid to prepare ZrB_2-SiC ceramics through reactive spark plasma sintering (R-SPS) at 1450 ℃. The sizes of ZrB_2 and SiC grains ranged from 80 to 350 nm with a uniform distribution of phases, due to the molecular homogeneity of $ZrSi_2$ and the homogeneous mixing of raw material powders. However, the impact of phase dimensions on oxidation resistance in multiphase UHTCs is unclear. Therefore, further studies are necessary to investigate the differences in oxidation behaviors of ceramics with smaller grain sizes prepared by the reaction compared to ceramics prepared directly using powders of UHTCs.

In this work, ZrB_2-SiC ceramics were produced by tape casting combined with reactive melt infiltration. The formation of ZrB_2 and SiC phases involves the reaction between $ZrSi_2$, B_4C, and C, as shown in the following formula:

$$2ZrSi_2 + B_4C + 3C = 2ZrB_2 + 4SiC \quad (1)$$

Then, the ZrB_2-SiC ceramics were further densified by reactive melt infiltration of Si. Meanwhile, as a control group, ZrB_2-SiC ceramics were prepared using ZrB_2 and SiC powders as raw materials by the same process as described above. The microscopic morphology and compositional distribution of the ceramics were firstly analyzed. Subsequently, the oxidation behavior of the ceramics was revealed by analyzing the evolution of the phase composition and microstructure during oxidation in air at 1600 ℃. The differences between oxidation behaviors of the two ceramics were also discussed.

1 Experimental

1.1 Materials and ceramics preparation

ZrB_2-SiC ceramics were produced by combining tape casting with reactive melt infiltration of Si, as schematically shown in Fig. 1.

$ZrSi_2$ (99.5%, <1 μm, Forsman, Beijing), B_4C (99.9%, 2–4 μm, Aladdin, Shanghai), carbon black (99.5%, 30 nm, Aladdin, Shanghai), ZrB_2 (99.5%, <1 μm, Shuitian, Shanghai) and SiC (99%, 0.5–0.7 μm, Aladdin,

Shanghai) were used as raw materials. The first step was to prepare slurry, *i.e.* $ZrSi_2$, B_4C and carbon black powders were added into a polyethylene jar at molar ratio of 2 : 1 : 3 (shown in Table 1), using ethanol, phenolic resin and polyvinyl butyral (PVB) as a solvent, binder, and pore-making agent, respectively. The mixture was ball milled for 12 h. The slurry was degassed under vacuum after ball milling. Subsequently, it was used for tape casting with the blade height set at 300 μm and the casting rate set at 100 mm/min. After tape casting, the film was air-dried at room temperature for 12 h. The dried film was cut into 60 mm × 60 mm sheets and then the sheets were laminated into a block about 4 mm thick. The block was heated to 700 ℃ and held for 1 h in flowing argon atmosphere for debinding, and then heated to 1500 ℃ and held for 1 h to produce ZrB_2 and SiC in the porous preforms *via* reaction formula (1). Finally, the porous preforms were held in vacuum at 1500 ℃ for 30 min for reaction melt infiltration, and the ceramics (referred to as ZBC ceramics) were prepared by the reaction of molten Si with pyrolysis carbon (from phenolic resin) to produce SiC. In this experiment, ceramics (referred to as ZS ceramics) were prepared using ZrB_2 and SiC powders at a molar ratio of 1 : 2 as raw materials, following the above steps.

1.2　Cyclic oxidation tests

The prepared ceramics were cut into samples with dimensions of 5 mm×5 mm×3 mm and then placed into a muffle furnace for high temperature oxidation. The temperature was increased to 1600 ℃ at rate of 5 ℃/min and held for 2 h. After natural cooling, the samples were removed and weighed. After recording the mass of each sample, the samples were returned to the muffle furnace and the above steps were repeated, and the oxidation cycle was repeated 5 times for total of 10 h. The mass change per unit surface area (ΔW) was calculated by the following formula:

$$\Delta W = \frac{m_1 - m_0}{S_0} \tag{2}$$

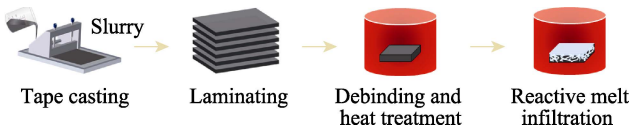

Fig. 1　Flow chart for the processing of ceramics

Table 1　Raw materials and their molar ratios for ceramics preparation

	ZBC			ZS	
Raw materials	$ZrSi_2$	B_4C	C	ZrB_2	SiC
Molar ratio	2	1	3	1	2

1.3　Characterization

The weight of the samples before and after the oxidation tests was recorded using analytical balance with accuracy of 0.01 mg. The average of 5 or more samples was calculated at each time. Phase compositions of the samples were characterized by X-ray diffraction (XRD, Ultima, IV, Rigaku Corporation, Kyoto, Japan, and D8 DISCOVER, Bruck, Germany) using Cu K_α radiation. The surface and cross-section microstructures of the samples were characterized by field emission scanning electron microscope (SEM, Magellan 400, FEI, USA), and the chemical compositions of the samples were characterized by equipped X-ray energy spectrometer (EDS, PN-5502, INCA ENGERY, UK). Some of the samples need to be metallurgically polished before characterization.

2　Results and analysis

2.1　Microstructure of ceramics

Fig. 2(a, b) show the XRD patterns and cross-sectional morphology of ZBC porous preforms after heat-treatment. As shown in Fig. 2(a), heat treatment of ZBC porous preforms can produce ZrB_2 and SiC. Fig. 2(b) shows that, besides ZrB_2 and SiC, the porous preforms contain pyrolysis carbon derived from phenolic resin, and these pyrolysis carbon would be used as carbon source to react with Si to form SiC in the reaction melt

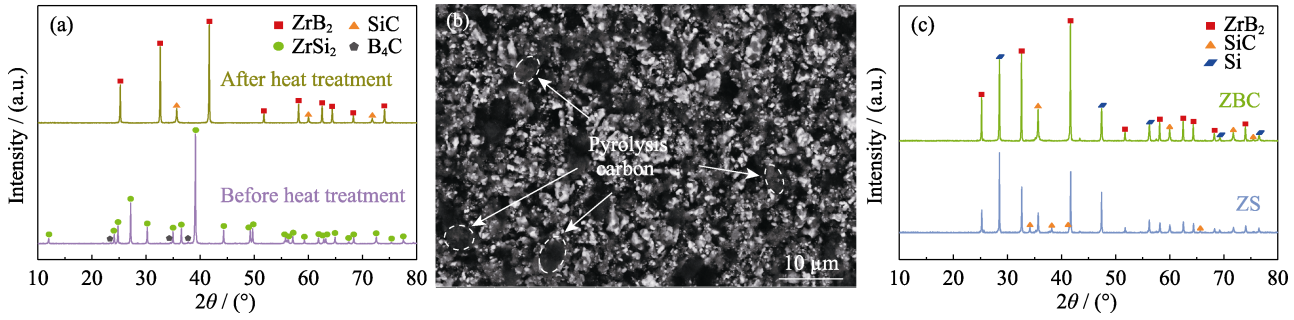

Fig. 2　Microstructure and morphology of ZBC samples

(a) XRD patterns of ZBC porous preforms before and after heat treatment; (b) Cross-sectional morphology of ZBC porous preforms after heat treatment; (c) XRD patterns of ceramics after reactive melt infiltration

infiltration process. Fig. 2(c) displays the XRD patterns of two ceramics ZBC and ZS. Both ceramics possess the same phases: ZrB_2, SiC and Si. Compared to Fig. 2(a), there is a significant increase in the intensity of the SiC peaks after reaction melt infiltration. This suggests that Si react with carbon to form SiC in the porous preforms during the reaction melt infiltration process. XRD patterns show Si peaks due to the presence of Si residue left by the reactive melt infiltration process.

Fig. 3 displays the surface and cross-sectional morphologies of the ZBC ceramics. Fig. 3(a-c) demonstrate that the surfaces of the ceramics have uniform compositional distribution and dense structure. Fig. 3(d-f) show that the cross-sections of the ceramics are still dense with no apparent delamination, indicating that the interlayer bonding of the ceramics is tight. Fig. 4 displays the surface and cross-sectional SEM morphologies of the ZS ceramics. It is seen that the morphology of ZS ceramics is similar to that of ZBC ceramics. But the particle size of ZrB_2 in ZS ceramics is larger than that in ZBC ceramics, indicating that the ZrB_2 produced through the reaction has a smaller particle size. Additionally, both Fig. 3 and Fig. 4 indicate that the ceramics mainly contain three phases. According to the EDS results, it can be inferred that the bright white region, gray region and black region are ZrB_2 (Spot 1, Spot 4), Si (Spot 2, Spot 5),

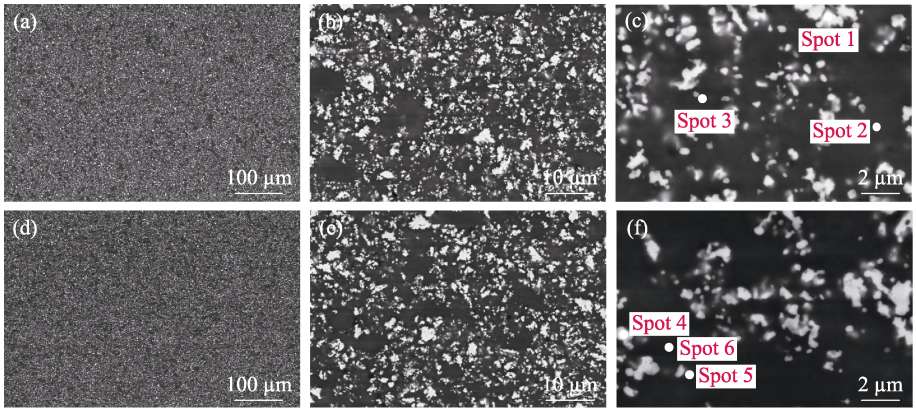

EDS/%(in atom)						
Element	Spot 1	Spot 2	Spot 3	Spot 4	Spot 5	Spot 6
Zr	40.81	–	–	40.80	–	–
B	59.19	–	–	59.20	–	–
Si	–	86.33	47.22	–	86.58	47.91
C	–	13.67	52.78	–	13.42	52.09

Fig. 3 Morphologies and corresponding EDS analyses of ZBC ceramics
(a-c) Surface; (d-f) Cross section

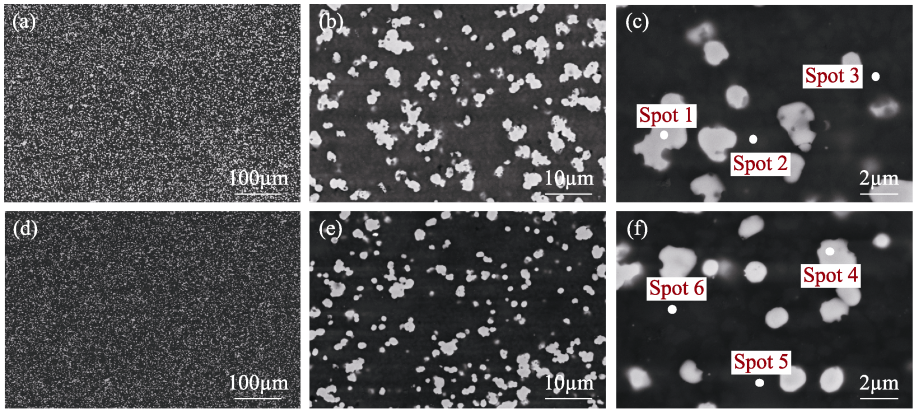

EDS/%(in atom)						
Element	Spot 1	Spot 2	Spot 3	Spot 4	Spot 5	Spot 6
Zr	40.15	–	–	40.49	–	–
B	59.85	–	–	59.51	–	–
Si	–	87.96	44.58	–	89.93	45.07
C	–	12.04	55.42	–	10.07	54.93

Fig. 4 Morphologies and corresponding EDS analyses of ZS ceramics
(a-c) Surface; (d-f) Cross section

SiC (Spot 3, Spot 6), respectively. This is consistent with the XRD patterns in Fig. 2(c).

2.2 Cyclic oxidation behavior of ceramics

Fig. 5 displays the XRD patterns of the ceramics after oxidation at 1600 ℃ in the air. Fig. 5 shows the intensity of the $ZrSiO_4$ peaks in ZS ceramics is more pronounced compared to ZBC ceramics. According to the binary phase diagram in Fig. 6[28], $ZrSiO_4$ is formed by the reaction of ZrO_2 with SiO_2. The oxidation process involves the following reactions:

$$Si(l)+O_2(g)=SiO_2(l) \quad (3)$$

$$2SiC(s)+3O_2(g)=2SiO_2(l)+2CO(g) \quad (4)$$

$$2ZrB_2(s)+5O_2(g)=2ZrO_2(s)+2B_2O_3(g) \quad (5)$$

$$SiO_2(s)+ZrO_2(s)=ZrSiO_4(s) \quad (6)$$

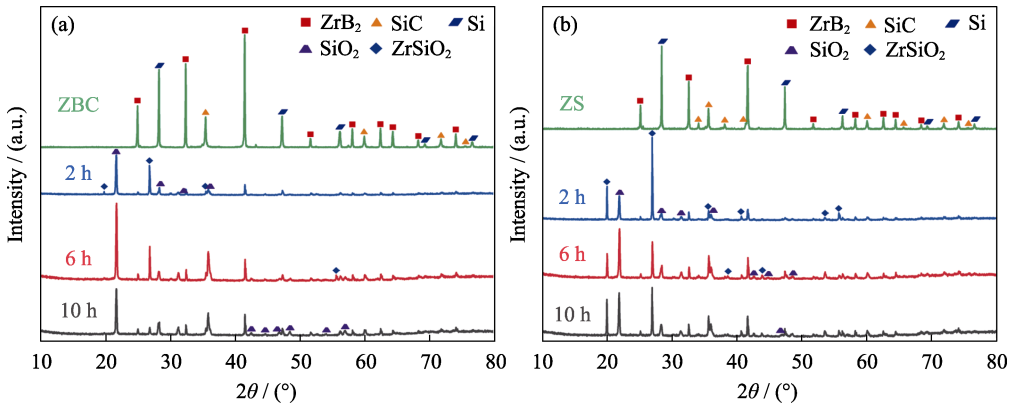

Fig. 5　XRD patterns of ceramics oxidized at 1600 ℃ in the air for different periods
(a) ZBC; (b) ZS

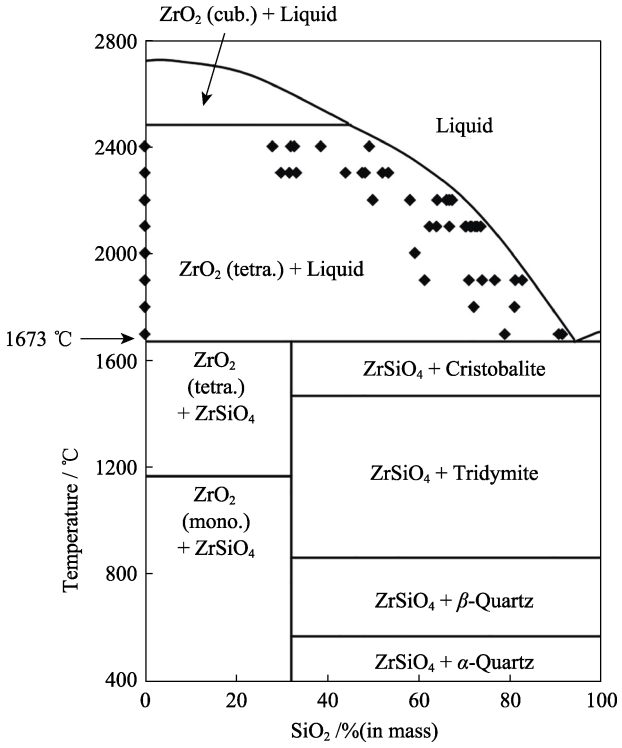

Fig. 6　ZrO_2-SiO_2 binary phase diagram[28]

Fig. 7 shows the surface morphology of ZBC ceramics after oxidation at 1600 ℃ in the air. Fig. 7(a-c) displays the surface morphologies of the ZBC ceramics after oxidation for 2 h. The surface of ZBC ceramics after oxidation displays three distinct zones: oxidation zone, transition zone, and slightly oxidized zone. According to EDS results, it can be inferred that the oxidation zone contains a significant quantity of $ZrSiO_4$ (Spot 1, Spot 5, and Spot 9). The transition zone contains precrystallization products with a dendritic structure. As revealed by EDS analysis, this structure is formed by the combination of ZrO_2 and SiO_2 at molar ratio less than 1 : 1 (Spot 6). The slightly oxidized zone is uniform with no cracks, and the EDS results indicate that this phase is SiO_2 with traces of ZrO_2 solidly dissolved (Spot 3). Fig. 7(d-f) displays the surface morphologies of the ZBC ceramics after oxidation for 6 h, which is similar to the morphology after oxidation for 2 h. The difference lies in the fact that the slightly oxidized zone is no longer homogeneous with a few cracks. With the oxidation time increasing to 10 h, the morphology of the slightly oxidized zone is gradually approaching the transition zone, and many cracks appear (Fig. 7(g-i)).

Based on the surface morphology evolution of the ZBC ceramics after oxidation for different time, it can be inferred that the ZBC ceramics undergo three stages during the oxidation process. During the first stage, SiC, Si, and ZrB_2 undergo oxidation to form SiO_2 and ZrO_2. As shown in Fig. 3, ZrB_2 particles are uniformly distribute between SiC and Si, resulting in a diffuse distribution of ZrO_2 between SiO_2. This leads to the formation of a SiO_2-ZrO_2 glassy oxide layer. During cooling, the edge region undergoes more severe oxidation, leading to a higher ZrO_2 content precipitating out of SiO_2. SiO_2 loses ZrO_2 and begins to crystallize, and forms a

eutectic with ZrO_2, leading to the formation of $ZrSiO_4$. This leads to cracking in the edge region due to the mismatch of the coefficients of thermal expansion. In the central region, SiO_2 remains in glassy state due to the high viscosity of the SiO_2-ZrO_2 oxide layer. During the second stage, as the number of cyclic oxidations increases, a small amount of ZrO_2 in the central region of the oxide layer migrates and enriches during the cooling process, eventually precipitating crystals in the region of higher concentration. At the same time, the loss of ZrO_2 causes crystallization of SiO_2. During the third stage, the number of cyclic oxidations continues to increase, causing a significant migration of ZrO_2 during the cooling process. Simultaneously, a considerable amount of SiO_2 begins to crystallize and forms a eutectic with ZrO_2, leading to the formation of $ZrSiO_4$, and ultimately resulting in cracks in the center region of the oxide layer.

Fig. 8 shows the surface morphology of ZS ceramics after oxidation at 1600 ℃ in the air. It indicates that the oxidation surface of ZS ceramics differs from that of ZBC ceramics. The surface of ZS ceramics exhibits numerous $ZrSiO_4$ particles. As the oxidation time increasing, cracks in the surface of ZS ceramics gradually widen and bubbles appear. Based on the results presented in Fig. 4, it is evident that the ZrB_2 particle size in ZS ceramics is large. As a result, the diffusion of ZrO_2 generated after oxidation in SiO_2 is difficult. Consequently, a high viscosity SiO_2-ZrO_2 glassy oxide layer is not formed, leading to a significant amount of SiO_2 crystallization during the cooling stage. Ultimately, it forms a eutectic mixture with ZrO_2, resulting in the creation of $ZrSiO_4$. This result is also consistent with the XRD pattern of Fig. 5(b).

Fig. 9 shows the cross-sectional morphologies of ZBC and ZS ceramics oxidized in the air at 1600 ℃. With the duration of oxidation, all ceramics show an increase of thickness of the oxide layer on the surface. Moreover, the thickening of the oxide layer oxidized from 2 h to 6 h is larger than that oxidized from 6 h to 10 h. After oxidation for 10 h, the oxide layer of the edge zone in ZBC ceramics (Fig. 9(c)) mainly contains three phases. Based on the EDS results, it can be inferred that the bright white region, gray region and black region are $ZrSiO_4$ (Spot 1), $9SiO_2$-ZrO_2 (Spot 2) and SiO_2 (Spot 3), respectively. The cross-sectional morphology of this zone corresponds to the oxidation and transition zone on the surface of ZBC ceramics in Fig. 7 due to the presence of obvious cracks in the oxide layer. Fig. 9(d-f) display the cross-sectional morphologies of the central zone of ZBC ceramics. The thickness of the oxide layer in the central zone is slightly thinner than that of the edge zone. After oxidation for 2 and 6 h, the oxide layer in the central zone still maintains dense and homogeneous morphology. After oxidation for 10 h, the oxide layer begins to

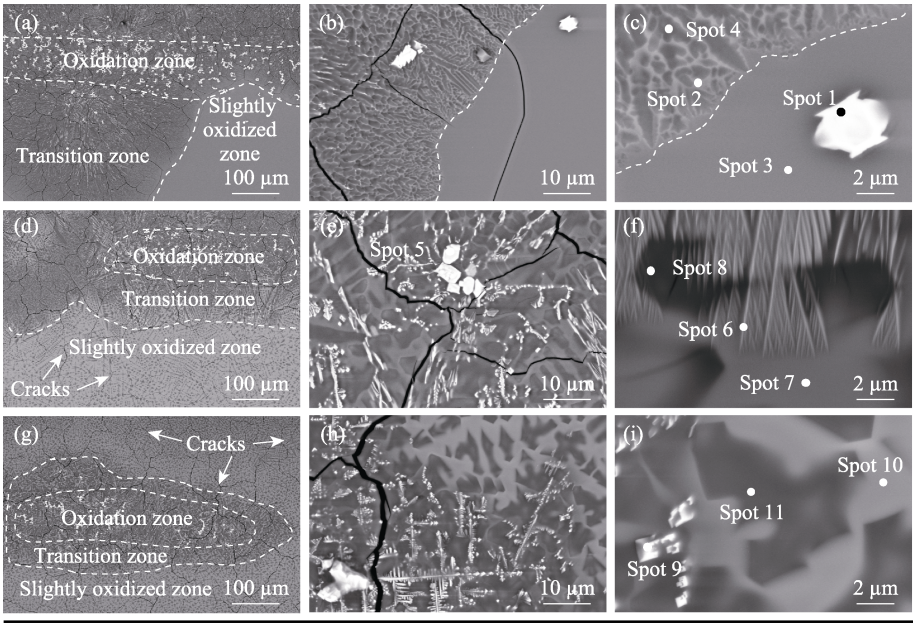

EDS/%(in atom)											
Element	Spot 1	Spot 2	Spot 3	Spot 4	Spot 5	Spot 6	Spot 7	Spot 8	Spot 9	Spot 10	Spot 11
Zr	16.42	3.72	1.42	–	16.20	8.88	3.29	–	13.59	3.30	–
Si	16.94	28.62	31.41	33.02	17.17	23.52	28.84	66.68	19.79	28.75	33.40
O	66.64	67.66	67.17	66.98	66.63	67.60	67.87	33.32	66.62	67.95	66.60

Fig. 7 Surface morphologies of ZBC ceramics oxidized at 1600 ℃ for different periods
(a-c) 2 h; (d-f) 6 h; (g-i) 10 h

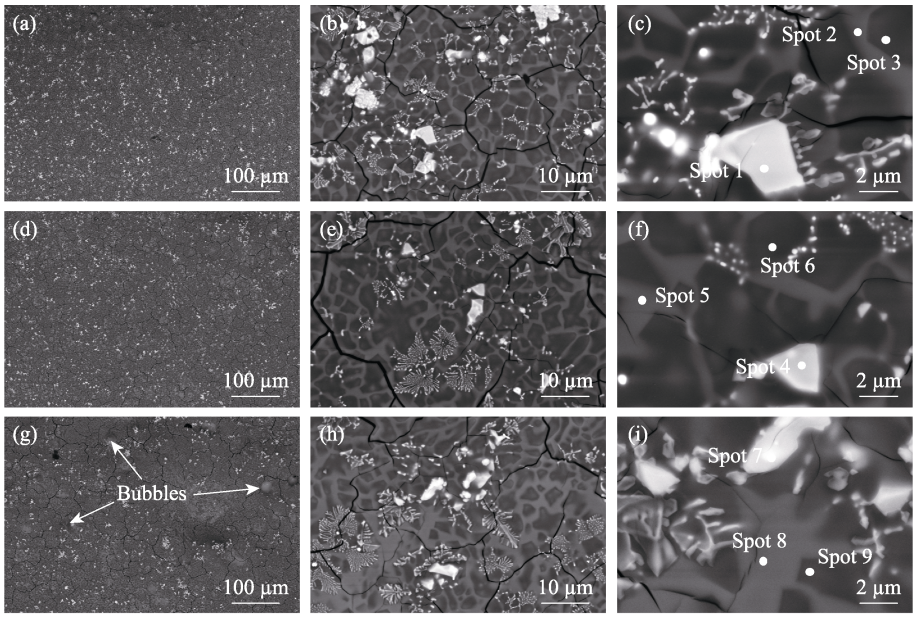

EDS/%(in atom)									
Element	Spot 1	Spot 2	Spot 3	Spot 4	Spot 5	Spot 6	Spot 7	Spot 8	Spot 9
Zr	15.95	0.97	–	16.26	0.94	–	17.17	1.91	–
Si	17.41	30.53	33.32	17.10	31.00	32.66	16.18	30.29	33.32
O	66.64	68.50	66.68	66.64	68.06	67.34	66.65	67.80	66.68

Fig. 8　Surface morphologies of ZS ceramics oxidized at 1600 ℃ for different periods
(a-c) 2 h; (d-f) 6 h; (g-i) 10 h

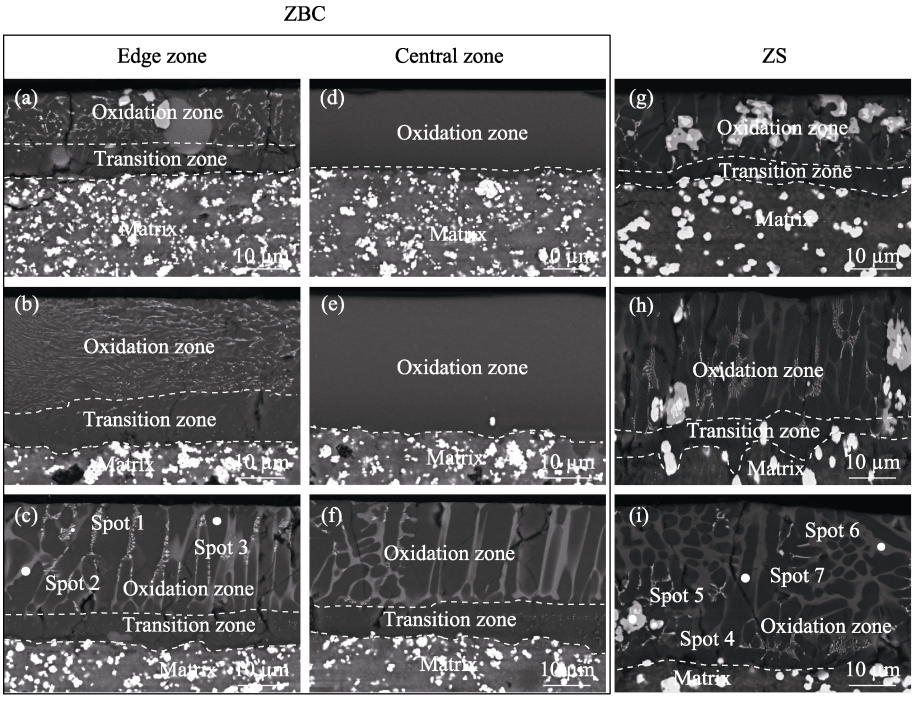

EDS/%(in atom)							
Element	Spot 1	Spot 2	Spot 3	Spot 4	Spot 5	Spot 6	Spot 7
Zr	15.03	3.49	–	33.63	16.50	2.57	–
Si	18.33	28.68	34.21	–	16.86	30.02	33.50
O	66.64	67.83	65.79	66.37	66.64	67.41	66.50

Fig. 9　Cross-sectional SEM morphologies of ceramics oxidized at 1600 ℃ for different periods
(a, d, g) 2 h; (b, e, h) 6 h; (c, f, i) 10 h

crystallize and a minor number of cracks appears. Therefore, the cross-sectional morphology of this zone corresponds to the slightly oxidized zone on the surface of ZBC ceramics in Fig. 7. Fig. 9(g-i) show the cross-sectional morphologies of ZS ceramics. Thickness of the oxide layer of ZS ceramics is greater than that of ZBC ceramics. According to the EDS results, the oxide layer mainly contains four phases: ZrO_2 (Spot 4), $ZrSiO_4$ (Spot 5), $10SiO_2$-ZrO_2 (Spot 6), and SiO_2 (Spot 7) correspond to bright white region, white region, gray region, and black region, respectively. After oxidation for 2 h, SiO_2 crystallizes in the oxide layer and a limited number of cracks appears. As oxidation time increasing, the thickness of the oxide layer also increases, and the cracks gradually expand. The cross-sectional SEM morphology of ZS ceramics is consistent with the results shown in Fig. 8.

The oxidation resistance can be evaluated quantitatively by analyzing the thickness of the oxide layer and the mass change during the oxidation process. Fig. 10 displays the thickness change of the oxide layer during the oxidation of ZBC and ZS ceramics. The thickness of the oxide layer increases rapidly in the first 6 h oxidation and then increases slowly in the following 4 h oxidation, exhibiting good oxidation resistance of the oxide layers of both ceramics. Furthermore, the thickness of the oxide layer of ZBC ceramics is thinner than that of ZS ceramics, which indicates that the former shows better oxidation resistance than the latter.

The mass change curves of two ceramics ZBC and ZS during the oxidation process are shown in Fig. 11. It shows that both ceramics gain weight more quickly in the first 6 h oxidation and slowly in the last 4 h oxidation. Additionally, the weight gain of ZS ceramics is higher than that of ZBC ceramics, which is consistent with the thickness variation of the oxide layer in Fig. 10. The experimental results indicate that the oxidation resistance of ZBC ceramics at 1600 ℃ is better than that of ZS ceramics. It can be concluded that the reaction of $ZrSi_2$, B_4C, and C results in the preparation of ZrB_2-SiC ceramics with fine particle size and homogeneous compositions, so that the ceramics exhibit superior high-temperature oxidation resistance.

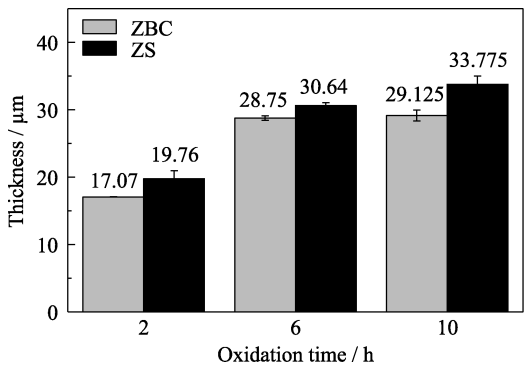

Fig. 10 Thickness of the oxide layer of ceramics oxidized at 1600 ℃ for different periods

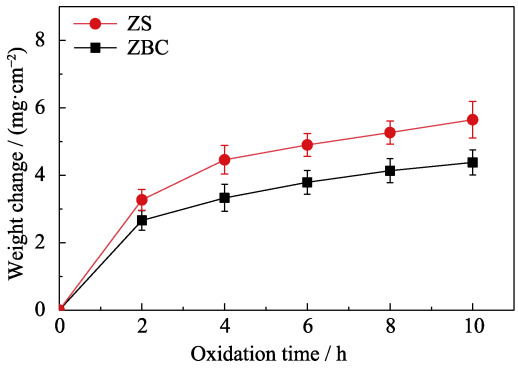

Fig. 11 Weight change curves of ZBC and ZS ceramics oxidized at 1600 ℃ for different periods

3 Conclusions

ZBC ceramics and ZS ceramics were produced *via* tape casting combined with reactive melt infiltration. ZBC ceramics were prepared by the reaction between $ZrSi_2$, B_4C and C, while ZS ceramics were prepared directly using ZrB_2 and SiC powders. The cyclic oxidation performance of two ceramics was evaluated at 1600 ℃. Following are some main conclusions:

Due to the small particle size of ZrB_2 in ZBC ceramics, the SiO_2-ZrO_2 oxide layer generated in the oxidation exhibits high viscosity. During the first three cycles of oxidation tests, the center region of the oxide layer remains the glassy state due to the high viscosity of the oxides. As a result, SiO_2 does not crystallize during the temperature reduction process. The edge region experiences severe oxidation, causing ZrO_2 to precipitate from the glassy SiO_2 due to the high content during the cooling process. As a result, SiO_2 loses ZrO_2, begins to crystallize and forms a eutectic with ZrO_2, leading to the formation of $ZrSiO_4$. This ultimately leads to cracking in the edge region due to the mismatch of the coefficients of thermal expansion. During the latter two cycles of the oxidation test, ZrO_2 migrates and enriches in the center region, causing SiO_2 to crystallize and have a eutectic with ZrO_2, resulting in the formation of $ZrSiO_4$. This ultimately leads to the development of cracks due to the difference in coefficients of thermal expansion. While for ZS ceramics, due to ZrB_2 particle size is large, after the first cycle oxidation test, the SiO_2 on the surface of the entire oxide layer begins to crystallize and eutectic react with ZrO_2 to produce $ZrSiO_4$, and finally produce many cracks due to the different coefficients of thermal expansion. It can be observed that the structure of the

ZBC ceramics is more stable exhibiting better oxidation resistance.

The oxidation rate of the ceramics is faster in the first 3 cyclic oxidation tests and becomes slower in the last 2 cyclic oxidation tests. The SiO_2-ZrO_2 oxide layer has demonstrated good resistance to oxidation. The thickness and mass increase of the oxide layer in ZBC ceramics are lower than that of ZS ceramics. Therefore, it can be concluded that the resistance to oxidation of ZBC ceramics, which are made from the reaction of $ZrSi_2$, B_4C, and C, is superior.

References:

[1] FU Q, ZHANG P, ZHUANG L, *et al*. Micro/nano multiscale reinforcing strategies toward extreme high-temperature applications: take carbon/carbon composites and their coatings as the examples. *Journal of Materials Science & Technology*, 2022, **96:** 31.

[2] ZHANG G J, NI D W, ZOU J, *et al*. Inherent anisotropy in transition metal diborides and microstructure/property tailoring in ultra-high temperature ceramics—a review. *Journal of the European Ceramic Society*, 2018, **38(2):** 371.

[3] THIMMAPPA S K, GOLLA B R, PPRASAD VVB. Oxidation behavior of silicon-based ceramics reinforced diboride UHTC: a review. *Silicon*, 2022, **14(18):** 12049.

[4] MUNGIGUERRA S, SILVESTRONI L, SAVINO R, *et al*. Qualification and reusability of long and short fibre-reinforced ultra-refractory composites for aerospace thermal protection systems. *Corrosion Science*, 2022, **195:** 109955.

[5] ZHANG P, FU Q G, CHENG C Y, *et al*. Microstructure evolution of *in-situ* SiC-HfB_2-Si ternary coating and its corrosion behaviors at ultra-high temperatures. *Journal of the European Ceramic Society*, 2021, **41(13):** 6223.

[6] VINCI A, ZOLI L, GALIZIA P, *et al*. Reactive melt infiltration of carbon fibre reinforced ZrB_2/B composites with Zr_2Cu. *Composites Part A: Applied Science and Manufacturing*, 2020, **137:** 105973.

[7] LEVINE S R, OPILA E J, HALBIG M C, *et al*. Evaluation of ultra-high temperature ceramics for aeropropulsion use. *Journal of the European Ceramic Society*, 2002, **22(14/15):** 2757.

[8] GOLLA B R, MUKHOPADHYAY A, BASU B, *et al*. Review on ultra-high temperature boride ceramics. *Progress in Materials Science*, 2020, **111:** 100651.

[9] OPEKA M M, TALMY I G, ZAYKOSKI J A. Oxidation-based materials selection for 2000 ℃+hypersonic aerosurfaces: theoretical considerations and historical experience. *Journal of Materials Science*, 2004, **39(19):** 5887.

[10] ZHANG S M, WANG S, LI W, *et al*. Microstructure and properties of W-ZrC composites prepared by the displacive compensation of porosity (DCP) method. *Journal of Alloys and Compounds*, 2011, **509(33):** 8327.

[11] LI K Z, SHEN X T, LI H J, *et al*. Ablation of the carbon/carbon composite nozzle-throats in a small solid rocket motor. *Carbon*, 2011, **49(4):** 1208.

[12] ZHANG Y L, HU H, ZHANG P F, *et al*. SiC/ZrB_2-SiC-ZrC multilayer coating for carbon/carbon composites against ablation. *Surface and Coatings Technology*, 2016, **300:** 1.

[13] YAN B, CHEN Z F, ZHU J X, *et al*. Effects of ablation at different regions in three-dimensional orthogonal C/SiC composites ablated by oxyacetylene torch at 1800 ℃. *Journal of Materials Processing Technology*, 2009, **209(7):** 3438.

[14] VERMA V, CHEVERIKIN V, CÂMARA COZZA R. Review: effect on physical, mechanical, and wear performance of ZrB_2-based composites processed with or without additives. *International Journal of Applied Ceramic Technology*, 2020, **17(6):** 2509.

[15] LIU Y J, ZU Y F, TIAN H L, *et al*. Microstructure and mechanical properties of continuous carbon fiber-reinforced ZrB_2-based composites *via* combined electrophoretic deposition and sintering. *Journal of the European Ceramic Society*, 2021, **41(3):** 1779.

[16] BALBO A, SCITI D. Spark plasma sintering and hot pressing of ZrB_2-$MoSi_2$ ultra-high-temperature ceramics. *Materials Science and Engineering: A*, 2008, **475(1/2):** 108.

[17] FAHRENHOLTZ W G, HILMAS G E, TALMY I G, *et al*. Refractory diborides of zirconium and hafnium. *Journal of the American Ceramic Society*, 2007, **90(5):** 1347.

[18] ZIMMERMANN J W, HILMAS G E, FAHRENHOLTZ W G, *et al*. Thermophysical properties of ZrB_2 and ZrB_2-SiC ceramics. *Journal of the American Ceramic Society*, 2008, **91(5):** 1405.

[19] REZAIE A, FAHRENHOLTZ W G, HILMAS G E. Oxidation of zirconium diboride-silicon carbide at 1500 ℃ at a low partial pressure of oxygen. *Journal of the American Ceramic Society*, 2006, **89(10):** 3240.

[20] ZOU J, ZHANG G J, HU C F, *et al*. Strong ZrB_2-SiC-WC ceramics at 1600 ℃. *Journal of the American Ceramic Society*, 2012, **95(3):** 874.

[21] NEUMAN E W, HILMAS G E, FAHRENHOLTZ W G. Mechanical behavior of zirconium diboride-silicon carbide-boron carbide ceramics up to 2200 ℃. *Journal of the European Ceramic Society*, 2015, **35(2):** 463.

[22] SILVESTRONI L, KLEEBE H J, FAHRENHOLTZ W G, *et al*. Super-strong materials for temperatures exceeding 2000 ℃. *Scientific Reports*, 2017, **7:** 40730.

[23] SILVESTRONI L, SCITI D. Effects of $MoSi_2$ additions on the properties of Hf- and Zr-B_2 composites produced by pressureless sintering. *Scripta Materialia*, 2007, **57(2):** 165.

[24] ZHAO L T, HOU C, JIN X C, *et al*. Oxidation behaviors of ZrB_2-SiC ceramics with different porosity. *Advanced Engineering Materials*, 2023, **25(8):** 20221313.

[25] SILVESTRONI L, MERIGGI G, SCITI D. Oxidation behavior of ZrB_2 composites doped with various transition metal silicides. *Corrosion Science*, 2014, **83:** 281.

[26] D'AMICO C, BIANCHI G, PADOVANO E, *et al*. Effect of ZrB_2 addition on the oxidation behavior of Si-SiC-ZrB_2 composites exposed at 1500 ℃ in the air. *Journal of Applied Biomaterials & Functional Materials*, 2018, **16(1):** 14.

[27] LEE S H, FENG L, BAE C J. Densification of ZrB_2-SiC nanocomposites prepared using $ZrSi_2$, B_4C, and C additives. *Journal of Materials Research*, 2017, **32(17):** 3302.

[28] YOSHIASA A, TOBASE T, ARIMA-OSONOI H, *et al*. High-temperature diffraction experiments and phase diagram of ZrO_2 and $ZrSiO_4$. *Zeitschrift Für Naturforschung B*, 2021, **76(10/11/12):** 591.

流延成型结合反应熔渗制备 ZrB_2-SiC 陶瓷及其微观结构与氧化行为研究

谭 敏[1,2], 陈小武[1,2], 杨金山[1,2], 张翔宇[1,2], 阚艳梅[1,2], 周海军[1,2], 薛玉冬[1,2], 董绍明[1,2]

(1. 中国科学院 上海硅酸盐研究所, 高性能陶瓷和超精密微结构国家重点实验室, 上海 200050; 2. 中国科学院大学 材料与光电研究中心, 北京 100049)

摘 要: ZrB_2基陶瓷通常需要在高温高压条件下才能烧结致密, 而利用反应熔渗 Si 的方式可在 1500 ℃制得 ZrB_2-SiC 致密陶瓷。相较于常规制备方法, 反应制备法更容易获得晶粒细小、成分均匀的超高温陶瓷相。本研究以 $ZrSi_2$、B_4C 和 C 为原料, 通过流延成型结合反应熔渗制备 ZrB_2-SiC 陶瓷(简称 ZBC 陶瓷)。此外, 还以 ZrB_2 和 SiC 为原料, 通过相同的工艺制备了一组 ZrB_2-SiC 陶瓷(简称 ZS 陶瓷)作为对比样品。对两组陶瓷的微观形貌进行表征, 发现 ZBC 陶瓷中 ZrB_2 相的颗粒尺寸较小且弥散分布在陶瓷中, 而 ZS 陶瓷中 ZrB_2 相的颗粒尺寸较大。在 1600 ℃空气环境中对两组陶瓷进行循环氧化测试, 总共循环氧化 5 次, 每次 2 h。分析两者的氧化行为, 发现 ZBC 陶瓷与 ZS 陶瓷在氧化过程中表面都会形成玻璃态 SiO_2-ZrO_2 氧化层, 起到阻隔氧气的作用。不同点在于 ZBC 陶瓷中 ZrO_2 弥散分布在 SiO_2 中, 而 ZS 陶瓷是大尺寸的 ZrO_2 与玻璃态 SiO_2 共存。在降温过程中, 弥散分布的 ZrO_2 能够提高玻璃态 SiO_2 的黏度, 抑制其结晶, 所以 ZBC 陶瓷的表面氧化层能够保持致密的结构; 而 ZS 陶瓷氧化层中 SiO_2 大量结晶并与 ZrO_2 共晶反应产生 $ZrSiO_4$, 由于热应力导致氧化层开裂, 使其阻隔氧气的作用大大减弱。分析两者的抗氧化性能, 发现 ZBC 陶瓷的氧化层厚度变化与质量增加均小于 ZS 陶瓷, 表明 ZBC 陶瓷的抗氧化性能优于 ZS 陶瓷。

关 键 词: 超高温陶瓷; ZrB_2-SiC; 氧化行为; 反应熔渗

中图分类号: TQ174 **文献标志码:** A **文章编号:** 1000-324X(2024)08-0955-10